https://doi.org/10.1007/s41230-023-2160-0

Interface characteristics and wear resistance of Ni-B_4C plated ZTA reinforced high chromium cast iron composite

Ke-liang Li[1, 2], **Wei Li[1, 2], and *Yan-liang Yi[1, 2]

1. Institute of Advanced Wear & Corrosion Resistant and Functional Materials, Jinan University, Guangzhou 510632, China

2. National Joint Engineering Research Center of High Performance Metal Wear Resistant Materials Technology, Jinan University, Guangzhou 510632, China

Abstract: A chemical composite plating of Ni-B_4C was used to prepare the surface-modified zirconia toughened alumina (ZTA) ceramic particles. The ceramic preforms were prepared by the plated ZTA and sodium silicate solution binder, followed by casting infiltration to prepare the ZTA particles reinforced high chromium cast iron (HCCI) composites. The result reveals that a distinct interface layer forms at the ZTA/HCCI interface, which consists of phases of ZrB_2, FeB, Fe_2B, and $NaSiO_4$. The interfacial wettability between ZTA and HCCI is improved by the diffusion and reaction of Ni and B_4C. The wear test reveals that the Ni-B_4C plated ZTA particles can effectively improve the wear resistance of the ZTA/HCCI composite, and the wear rate of the composite is decreased to 11.6% of HCCI.

Keywords: ZTA; composite; high chromium cast iron; interface layer; three-body abrasive wear

CLC numbers: TG143 **Document code:** A **Article ID:** 1672-6421(2023)03-253-10

1 Introduction

Particle reinforced metal matrix composites (PRMMCs) are commonly utilized in applications such as coal mining, construction, transportation, as well as other applications [1-3]. Recently, zirconia toughened alumina (ZTA) ceramic particles reinforced metal matrix composites (ZTA-PRMMCs) have attracted wide attention. During the process of ZTA, the phase transition of ZrO_2 improves the fracture toughness, strength, hardness, and high-temperature performance of Al_2O_3 ceramics [4, 5]. Previous research on the ZTA-PRMMCs mainly focuses on material preparation, interfacial bonding, service performance, and so on. Dong et al. [6] prepared ZTA particles reinforced high chromium cast iron (HCCI) composites by shoot mixing and pressure compositing, achieving strong interface bonding between the HCCI matrix and ZTA particles without extra wettability pretreatment. AIA [7] prepared a preformed block using ZTA ceramic particles mixed with carbide particles and fine-grained Al_2O_3 powder. The block was placed on the workpiece's surface, followed by casting and infiltration to form ZTA reinforced composite. Ma et al. [8] prepared ZTA particles using the powder sintering, and the wear resistance performance of this ZTA particles reinforced gray iron matrix composites was enhanced by 2.7 times compared to the gray cast iron.

The high hardness and toughness of ZTA ceramic provides excellent wear resistance. Consequently, if ZTA particles are used as reinforcements for iron matrix composite, the ZTA particles reinforced iron matrix composite will perform with excellent wear resistance. However, the interfacial wettability between ZTA particles and iron matrix is poor. For example, the wetting angle between ZTA and HCCI reaches 102.3° [9], which leads to poor bonding between the metal and ceramic interface. Solving the interface wettability between ZTA particles and iron matrix is still one of the research difficulties of ZTA ceramic particles reinforced iron matrix composites. It has been demonstrated that element Ni cannot chemically

***Yan-liang Yi**

Male, born in 1989, Ph.D, Associate Professor. His main research interests are focused on material tribology, advanced metal material preparation and processing, laser surface treatment. To date, he has published more than 60 papers, including 34 papers as first author or corresponding author.

E-mail: y_yanliang@163.com

****Wei Li**

Male, born in 1963, Ph.D, Professor. His research interests include wear and corrosion resistant metal materials and their metal matrix composites, metal material preparation and material processing engineering, special functional metal materials and their metal matrix composites.

E-mail: liweijn@aliyun.com

Received: 2022-11-08; Accepted: 2023-04-16

react with HCCI, but can improve the wettability of ceramics and metals by solid solution with Fe atoms [10, 11]. B_4C has good compatibility and wettability with steel liquid [12], and the wettability angle of ZTA with B_4C layer and HCCI can be decreased to 64.25° [13]. At high temperatures, B_4C reacts with Fe to form FeB and Fe_2B, both of which have good wear resistance [14, 15]. When the temperature exceeds 1,450 °C, B_4C reacts with ZrO_2 to form ZrB_2 [16]. The wettability of ZrB_2 and Fe is excellent. And element Fe exhibits a good spreading degree on ZrB_2 substrate in argon-protected high-temperature environment, with a measured wettability angle of 50° [17]. As a result, it is a reasonable prediction that combining Ni and B_4C to improve the wettability of ZTA with iron will bring positive performances.

When ZTA is directly compounded with the iron matrix, the interface between ZTA and the matrix is mechanically bonded, and the overall performance of the composite will be weakened due to insufficient bonding strength. In this study, ZTA ceramic particles were plated with Ni-B_4C, followed by casting and infiltration into ZTA/HCCI composites. The design of Ni-B_4C plating was to achieve chemical combination of ZTA/HCCI interface. Finally, the influence mechanism of Ni-B_4C plating on the wear resistance of ZTA/HCCI composite was analyzed.

2 Experimental methods

2.1 Materials

The ZTA particles used were ZA40, obtained from Sicheng Grinding Technology Co., Ltd. (Zhengzhou city, Henan province, China). The main phase is α-Al_2O_3, the secondary phase is monoclinic ZrO_2, and the rest is a few glass phases, as indicated in Table 1 (provided by the Sicheng Grinding Technology Co., Ltd.). The particle size of ZTA ceramic is 2.36–3.35 mm. The ZTA ceramic was prepared through high-temperature sintering and crushing, as shown in Fig. 1. The corresponding physical and mechanical properties of the ZTA ceramic are listed in Table 2 [18].

The matrix material is lumpy HCCI, obtained from Shaoguan Qujiang Jinyang Wear Resistant Materials Co., Ltd. in Shaoguan city, Guangdong province, China. Its chemical composition is displayed in Table 3.

2.2 Composite

Ni-B_4C composite was plated on ZTA particles, with the following process: alkali washing (40 g·L^{-1} NaOH+8 g·L^{-1} Na_2SiO_3+8 g·L^{-1} Na_3PO_4+8 g·L^{-1} Na_2CO_3)→water washing 3 times→acid washing (6 mol·L^{-1} HCl)→water washing 3 times→sensitization (25 g·L^{-1} $SnCl_2$+2 mol·L^{-1} HCl) →activation (0.25 g·L^{-1} $PdCl_2$+0.5 mol·L^{-1} HCl) →composite plating.

Table 4 shows the constitution of the Ni-B_4C composite plating solution. The plating was carried out at 85 °C for 2, 4, 6, and 8 h, respectively. The stirring was carried out in the plating process. After plating, the ZTA particles were cleaned and dried. Figure 2(a) depicts the macroscopic morphology of the plated ZTA particles, which has a dark gray metallic luster on the surface.

Table 1: ZTA chemical composition

Composition	Al_2O_3	ZrO_2	TiO_2	Fe_2O_3	SiO_2
wt.%	55–57	35–44	≤1.5	≤0.5	≤1.0

Fig. 1: ZTA ceramic particles

Table 2: Physical and mechanical properties of ZTA [18]

Material	Grain size (μm)	Real density (g·cm^{-3})	Bulk density (g·cm^{-3})	Melting point (°C)	Hardness (GPa)
ZTA	23	4.6	1.9–2.3	1,890	19

Table 3: Main chemical composition of HCCI

Element	C	Cr	Mn	Si	Ni	Mo	Fe
wt.%	3.0–3.2	23–26	0.8–1.2	0.5–0.6	0.3–0.5	0.3–0.5	Bal.

Table 4: Constitution of Ni-B_4C composite plating solution (g·L^{-1})

$NiSO_4$	NaH_2PO_2	CH_3COONa	NaF	H_3PO_3	Succinic acid	$(NH_4)_2MoO_4$	KIO_3	SDS	Nano-B_4C
30	30	30	1	6	6	0.04	0.02	0.2	5

The plated ZTA particles (mass M) and the sodium silicate binder (10mass% M) were uniformly mixed. Subsequently, the particles were pressed into a metal mold, followed by heating to 70 °C for 6 h in a drying oven to prepare a ceramic preform [Figs. 2(b and c)]. During the heating process, the particles were strongly bonded through the reaction of $Na_2SiO_3+CO_2+H_2O=H_2SiO_3+Na_2CO_3$. The ZTA/HCCI composite was prepared by non-pressure casting and infiltration technique. A molten HCCI liquid (1,550 °C) was poured into a sand mold into which preforms were placed, and then cooled to room temperature. The morphology of ZTA particles-reinforced HCCI matrix composite is shown in Fig. 3.

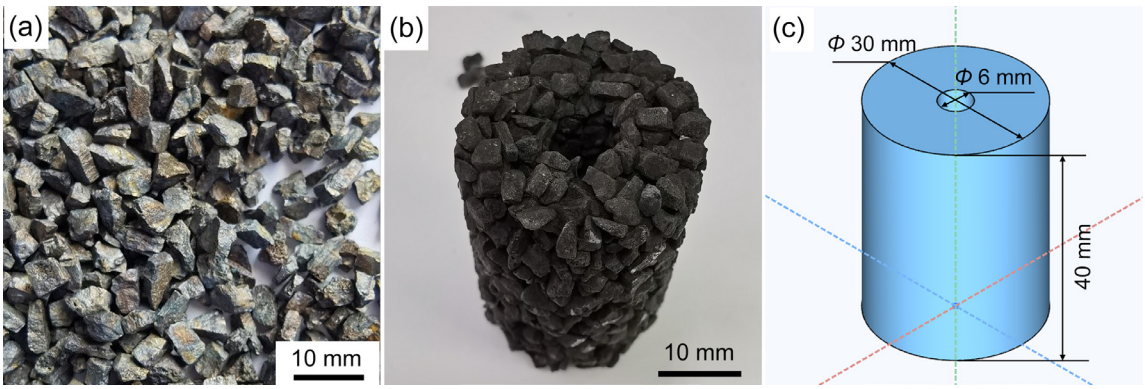

Fig. 2: ZTA ceramic particles coated with Ni-B_4C (a), ZTA preform (b), and ZTA preform size (c)

Fig. 3: Morphology of ZTA particles-reinforced HCCI matrix composite

2.3 Characterization

The composites were cut and sampled from the upper position of the casting at the same height. Microstructure morphology of the composites was observed using a DM3000 Leica optical microscope and a Thermo Scientific Apreo 2S scanning electron microscope. Phase constitutions were analyzed by a Ultima IV X-ray diffractometer using Cu-Kα at tube voltage 40 kV and tube current 40 mA, with scanning range 10°–90°, scanning speed 2°·min^{-1} and step 0.02°. Elemental distribution at the interface of the composites was characterized by a JXA-iHP200F field emission electron probe micro analyzer (EPMA parameters: electron gun acceleration voltage 30 kV, point resolution 1 nm, vacuum 10^{-4}–10^{-2} Pa). Gibbs free energy difference ΔG of relevant reactions was calculated by using the thermochemical software HSC Chemical 9 from Metso Outotec. Keysight Nano Indenter G200 nanoindenter was used to test hardness and elastic modulus.

2.4 Three-body abrasive wear

The MMH-5 three-body wear tester was selected for the wear test of pure HCCI and ZTA/HCCI composite. The wear principle is shown in Fig. 4(a), and the size of wear specimens is shown in Fig. 4(b). The abrasive material was #6 quartz sand, the spindle speed was 30 r·min^{-1}, the duration of a single test was 30 min, and the load was 40 N. After the wear test, the specimens were cleaned by high-frequency vibration in anhydrous ethanol, and then dried and weighed. The wear surface morphology of the wear specimen was characterized by 3D laser morphology analysis through an RTEC multifunctional testing machine.

The wear test was repeated three times and the average value was taken as the final result. The mass loss method is more suitable for evaluating the wear resistance of homogeneous materials, and the volume loss method is more suitable for evaluating the wear resistance of composites with large differences in component density. As a result, the volume loss was used to evaluate the wear resistance of pure HCCI and ZTA/HCCI composite, which can be calculated as follows [19]:

$$V_{loss}=M_{loss}/(\alpha\cdot\rho_p+(1-\alpha)\cdot\rho_m) \quad (1)$$

where V_{loss} is the volume loss, M_{loss} is the mass loss, α is the ceramic volume, ρ_p is density of ZTA ceramic, and ρ_m is the density of the HCCI.

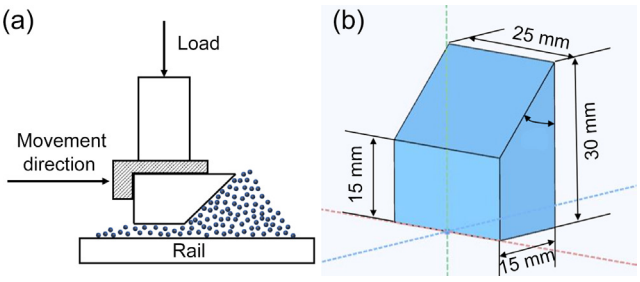

Fig. 4: Principle of three-body wear testing (a), and wear specimen size (b)

3 Results and discussion

3.1 Interfacial morphology of Ni-B_4C composite plating

Figure 5 shows the surface morphology and corresponding EPMA results of original ZTA and after 8 h Ni-B_4C plating. As shown in Fig. 5(a), the surface of the original ZTA particle is relatively smooth and flat. Zr, Al, and O are distributed on the surface of ZTA, which is consistent with the chemical composition of ZTA (Table 1). The surface morphology of Ni-B_4C plating exhibits a tiny granular structure, as illustrated in Fig. 5(b). The reason is that the nano-B_4C particles dynamically collide with the Ni atoms, causing the nano-B_4C particles to be fixed on the surface of the ZTA particles, resulting in the formation of a granular structure. The granular structure may be a microstructure of mixed nanocrystalline and amorphous [20]. Furthermore, the EPMA result reveals that the Ni, B, and C elements uniformly distribute on the surface of the plated ZTA, showing an effective chemical plated layer on the ZTA surface.

To gain a more direct understanding of the relationship between plating time and thickness of the plating layer, the cross-section morphologies of the ZTA particles with different plating times are shown in Fig. 6. The thickness of the plating layer was measured and averaged through 20 images, and the results are shown in Fig. 7. It can be seen that the growth rate of plating thickness increases firstly and then decreases. When the plating time reaches 6 h, the growth rate of the plating thickness begins to trend towards zero. Thus, the plating duration is set to 6 h, and the corresponding plated ZTA particles are obtained and used to prepare the performs and composite in this study.

To more directly observe the degree of interface bonding, the SEM morphology and corresponding EPMA analysis of a relatively thick plating layer (plating for 8 h) are shown in Fig. 8. It can be observed that the layer is uniform without obvious holes, cracks, or other defects. This indicates that the layer is tightly bonded, showing a good chemical plating effect.

3.2 Morphology of ZTA/HCCI composite

Figure 9(a) depicts the macroscopic morphology of the composite, where the gray-brown particles are ZTA particles and the silvery metal is HCCI. The volume percentage of ZTA

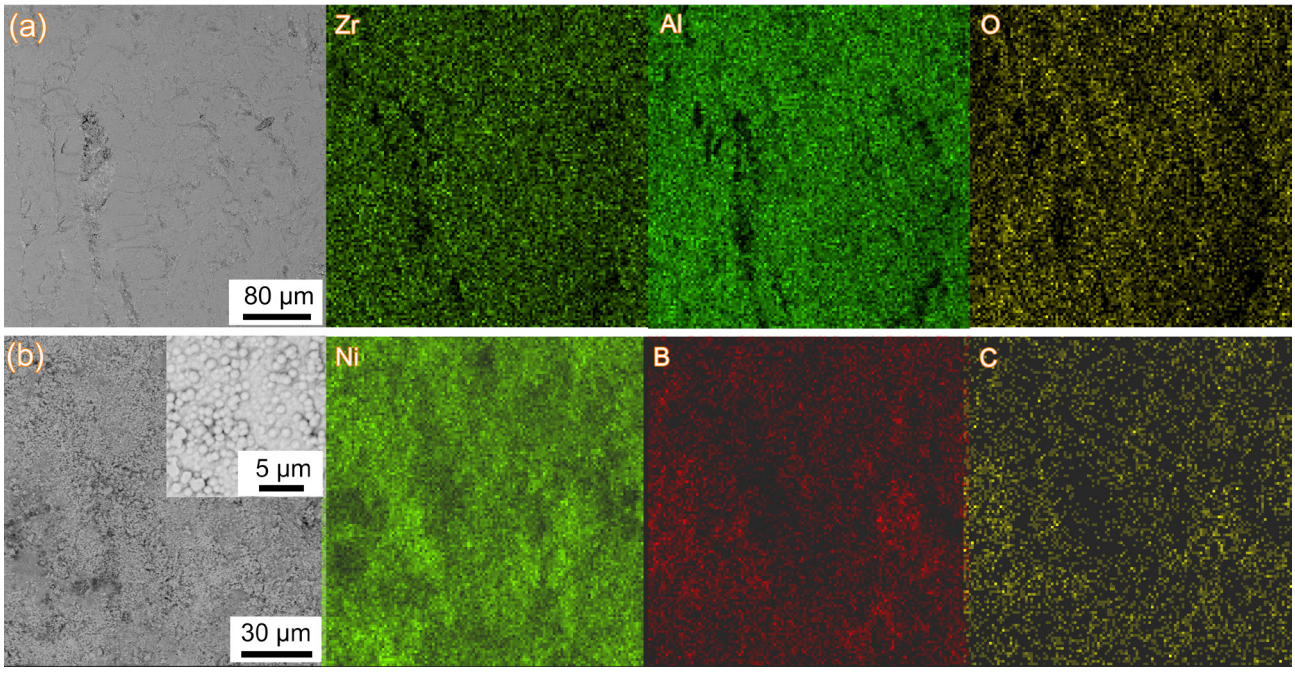

Fig. 5: Original ZTA surface morphology and corresponding EPMA results (a), and ZTA surface morphology after 8 h Ni-B_4C plating and corresponding EPMA results (b)

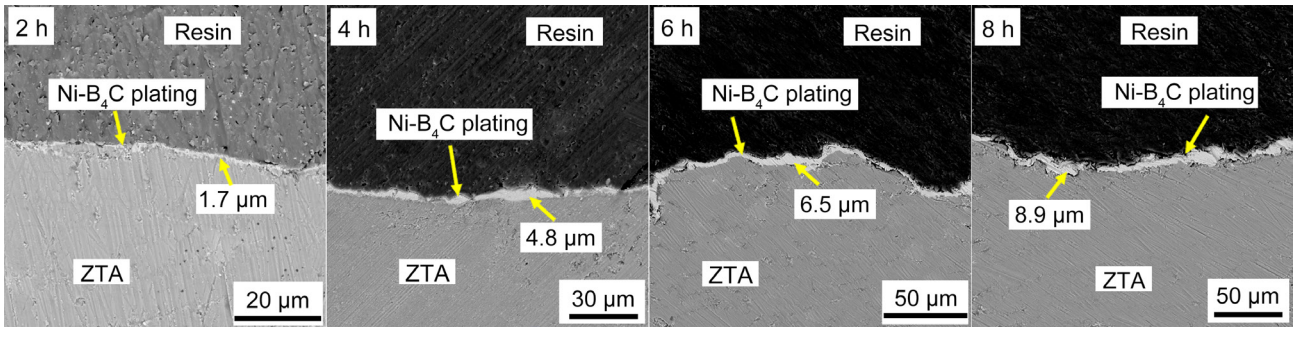

Fig. 6: Cross-section of ZTA particles with different plating times

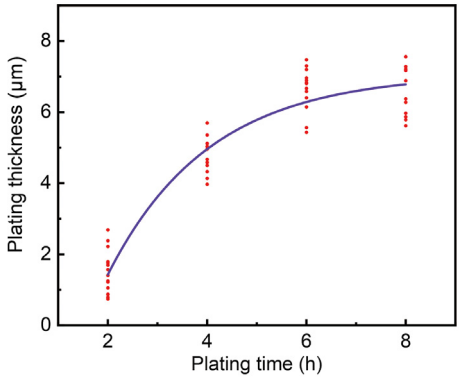

Fig. 7: Relationship between plating time and thickness of plating layer

ceramics in composite is about 45% (calculation method: cut 5 samples at the same height of the casting, use the area statistics function of the ImageJ software to count the percentage of ZTA ceramics in each of the 5 samples, and take the average value as the final value). The ZTA particles are evenly dispersed, and there are no visible casting defects in the composite. The result indicates that the preform is tightly bonded and the high chromium cast iron liquid can be effectively infiltrated into the ZTA preform. The microstructure morphology of the composite at the interface is shown in Fig. 9(b). No cracks appear at the ceramic/metal interface, and a distinct interface layer is formed at the interface. This indicates that the metal matrix is tightly bonded with the ZTA particles.

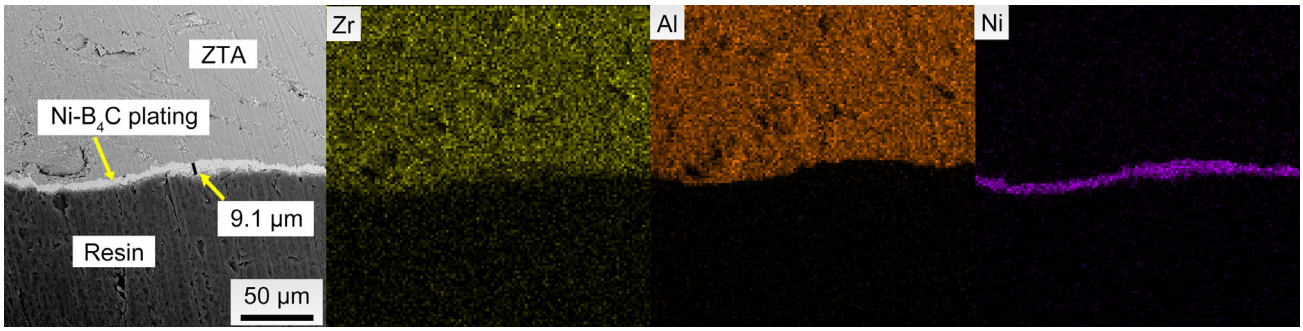

Fig. 8: Cross-section and corresponding EPMA analysis of ZTA particles plated by Ni-B_4C for 8 h

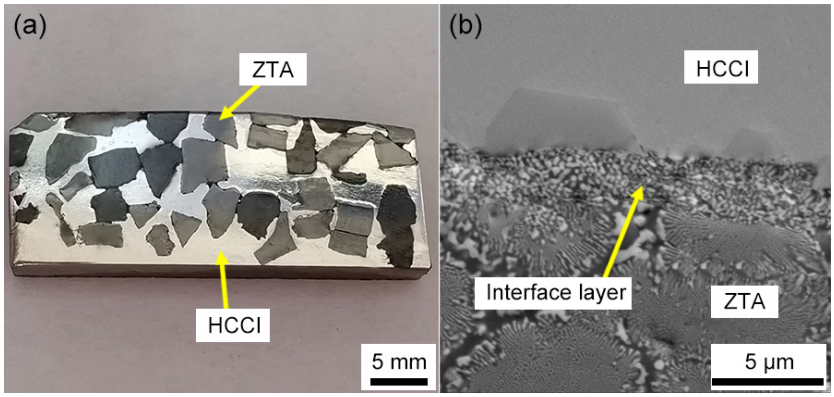

Fig. 9: Macroscopic (a) and micromorphologies (b) of ZTA/HCCI composite

3.3 Analysis of ZTA/HCCI interface characteristics

The reaction equation at the interface is as follows:

$$B_4C+4Fe=4FeB+C \quad (2)$$

$$B_4C+8Fe=4Fe_2B+C \quad (3)$$

$$B_4C+2ZrO_2+3C=4CO\ (g)+2ZrB_2 \quad (4)$$

The composite was prepared by using the casting and infiltration technique at about 1,550 °C. Thermodynamic calculations were solved to determine whether the foregoing chemical reactions can react at this temperature, and the results are shown in Fig. 10. The Gibbs free energy difference ΔG of the three chemical reactions is less than zero when the temperature exceeds 1,450 °C. This result indicates that all the three reactions can react spontaneously in this temperature range, with a high probability of forming new phases FeB, Fe_2B, and ZrB_2 at the ZTA/HCCI interface.

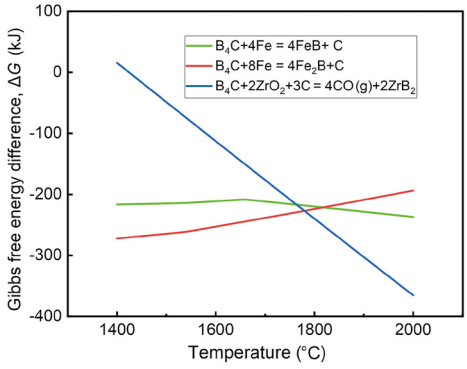

Fig. 10: Gibbs free energy difference ΔG for B_4C-related reactions

Figure 11 shows interface morphology and corresponding EPMA results of the ZTA/HCCI composite. It can be seen there is an uniform interface layer between ZTA and HCCI. This indicates that ZTA is tightly bonded with HCCI during the casting and infiltration process. Figure 12 shows XRD patterns of ZTA/HCCI composite's surface, which will be used to analyze the phase constitution of the composite materials.

EPMA energy spectrum shows that those dark gray areas are mainly composed of C, Fe, and Cr. Combined with the XRD pattern (Fig. 12), it can be inferred that this is the common carbide $(Cr, Fe)_7C_3$ in high chromium cast iron. In addition, the interface layer exists obvious element Si [Fig. 11(a)], which is known to originate from the $NaSiO_4$ phase based on the XRD pattern in Fig. 12. The $NaSiO_4$ phase originates from the sodium silicate binder added during the preparation of the preform.

The elements Zr and O also diffuse obviously in the interface layer (Fig. 11), which indicates that the diffusion of ZrO_2 from ZTA into the interface layer is achieved. Furthermore, the results of the line scanning show that there is a certain concentration of Zr elements in the interface layer [Fig. 11(b)], which indicates that $B_4C+2ZrO_2+3C=4CO\ (g)+2ZrB_2$ can occur. Consequently, it can be inferred that the formation of ZrB_2 phase in the interface layer is possible, which is verified by the results of XRD pattern in Fig. 12.

The element B in the composite interface comes from the 6 h Ni-B_4C plating, and the average thickness of the 6 h Ni-B_4C plating layer is about 6 μm (Fig. 7). This means that the amount of B_4C is small. As a result, it can be found that the detection amount of element B is low at the interface layer in Fig. 11. Another important reason is high compatibility between molten iron with B_4C. The B_4C will rapidly decompose and react with Fe atoms to generate FeB and Fe_2B at high temperatures. The XRD patterns in Fig. 12 reveal the presence of FeB and Fe_2B phases in the composite. As a result, the interface layer comprises a minor quantity of FeB and Fe_2B phases.

According to the EPMA energy spectrum shown in Fig. 11, Ni has a more uniform distribution in the metal matrix. Ni and Fe atom can replace each other to form a substitutional solid solution Ni-Fe [21]. Ni-Fe phases are found in the composites by XRD pattern, as shown in Fig. 12, which is the result of Ni element diffusion.

Based on the discussion above, B_4C in the Ni-B_4C plating layer will react with ZrO_2 to form ZrB_2, and with Fe to form FeB, Fe_2B, while the Ni elements will diffuse in the metal matrix to form Ni-Fe solid solution. As a result, the diffusion and reaction of Ni and B_4C will cause the Ni-B_4C plating layer to decompose. This is the reason why the average thickness of the interface layer 4.6 μm (Fig. 11) is less than that of the 6 h Ni-B_4C plating layer 6 μm on ZTA particles (Fig. 7).

The diffusion of Ni can decrease the wettability angle of ZTA and HCCI from 102.3° to 88.2° [9], and the wettability angle of B_4C plated ZTA and HCCI can be decreased to 64.25° [13]. Additionally, the wettability angle between ZrB_2 and Fe can reach 50° [17], FeB and Fe_2B are compatible with Fe [22]. This indicates that the diffusion and reaction of Ni and B_4C can effectively improve the interfacial wettability between ZTA and HCCI. In this study, an interface layer, which is comprised of ZrB_2, FeB, Fe_2B, and $NaSiO_4$, is formed between ZTA and HCCI by the diffusion and reaction of Ni and B_4C. As a result, the interfacial wettability between ZTA and HCCI is improved by the interface layer.

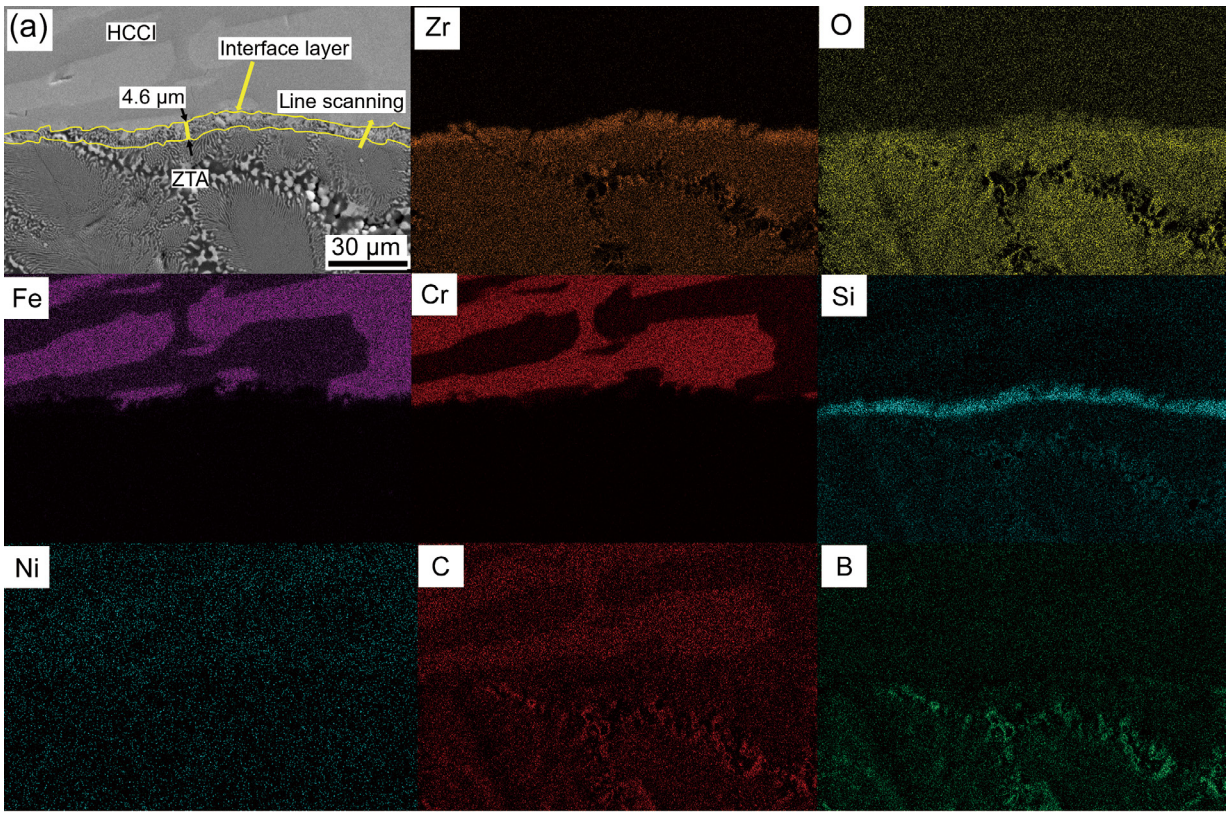

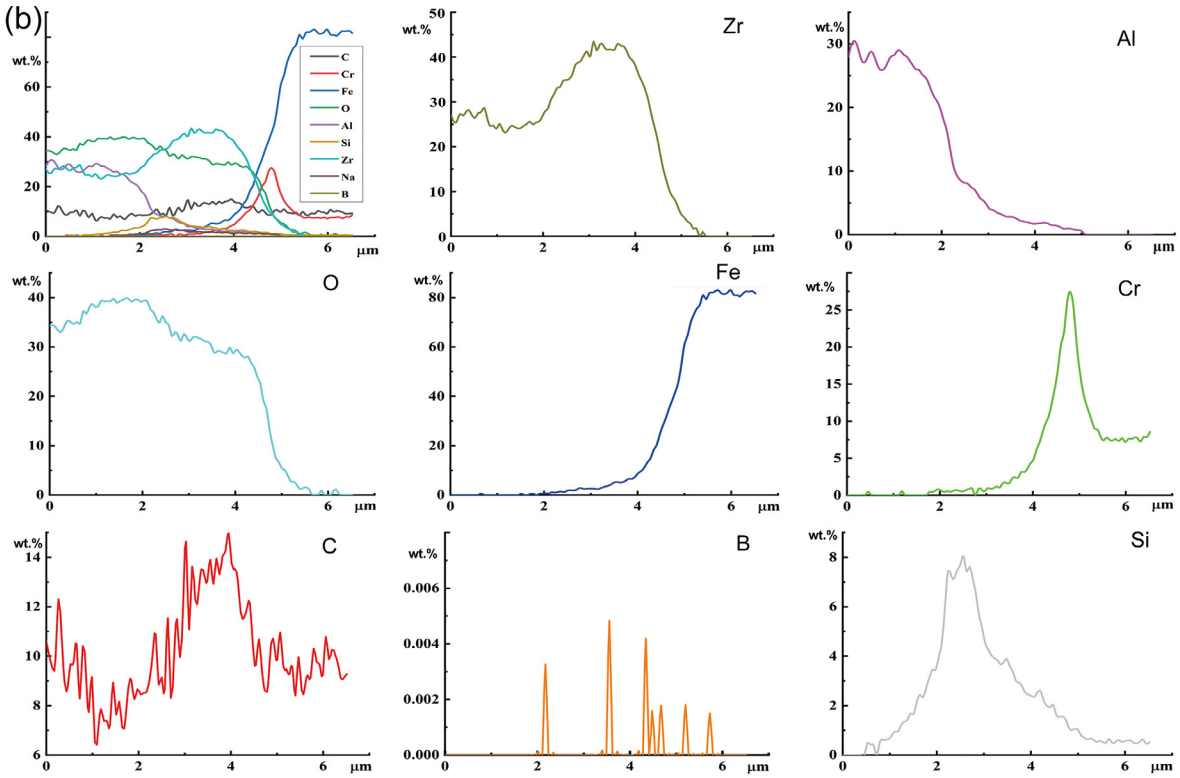

Fig. 11: EPMA surface scanning of composite (a), and line scanning at ZTA/HCCI interface (b)

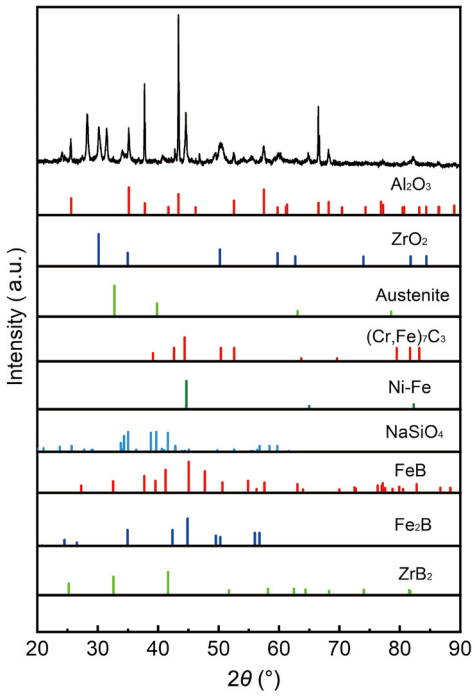

Fig. 12: XRD diffraction patterns of ZTA/HCCI composites

3.4 Hardness & elastic modulus

Figure 13 depicts the hardness and elastic modulus of the HCCI matrix, interface layer, and ZTA, and the distance between each value point is 50 μm. According to Fig. 13(a), the hardness of the matrix, interface layer, and ZTA is approximately 5.5 GPa, 4 GPa, and 20 GPa, respectively. The matrix hardness is approximately 33% greater than the interface layer, indicating that the interface layer is relatively soft. According to Fig. 13(b), the elastic modulus of the matrix, interface layer, and ZTA are approximately 222 GPa, 82 GPa, and 337 GPa, respectively. Matrix's elastic modulus is 1.7 times that of the interface layer, while the ZTA's elastic modulus is 3.1 times that of the transition zone. The elastic modulus reflects the material's ability to resist deformation when subjected to an external force [23]. The interface layer is more ductile and prone to plastic deformation, which will reduce stress concentration around particles and aid in load transfer [24]. Consequently, the interface layer with a relatively low hardness and elastic modulus is a benefit to the transfer and buffering of energy load between the ZTA/HCCI interface, which probably has a positive effect on the improvement of the composite's wear resistance.

3.5 Wear resistance of ZTA/HCCI composites

The results of three-body wear test for HCCI and ZTA/HCCI composites are shown in Fig. 14. As previously stated, there is a relatively soft interface layer between the composite's ZTA/HCCI interface. This interface layer not only increases wettability between ZTA and HCCI, but also contributes to load transmission between ZTA and HCCI. Thus, the three-body wear resistance of the composites is significantly stronger than that of pure HCCI. At a wear time of 30 min, the volume loss ratio of pure HCCI specimen to ZTA/HCCI composite is approximately 2.48. When the wear time is 180 min, the wear volume loss of the pure HCCI specimen is 1,009.97 mm^3, while that of the composite is 144.55 mm^3, and the wear volume loss ratio of pure HCCI and ZTA/HCCI composite is approximately 6.99. According to Fig. 14(b), the wear rates of HCCI and composite are 5.6 $mm^3 \cdot min^{-1}$ and 0.65 $mm^3 \cdot min^{-1}$, respectively.

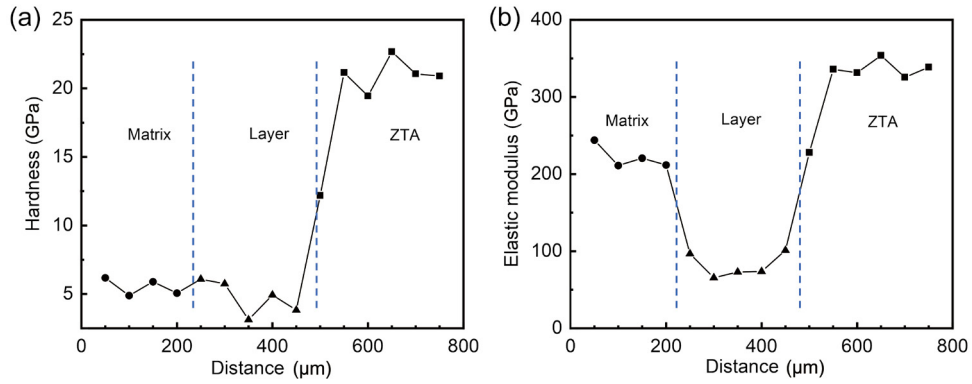

Fig. 13: Hardness (a) and elastic modulus (b) of matrix, interface layer, and ZTA

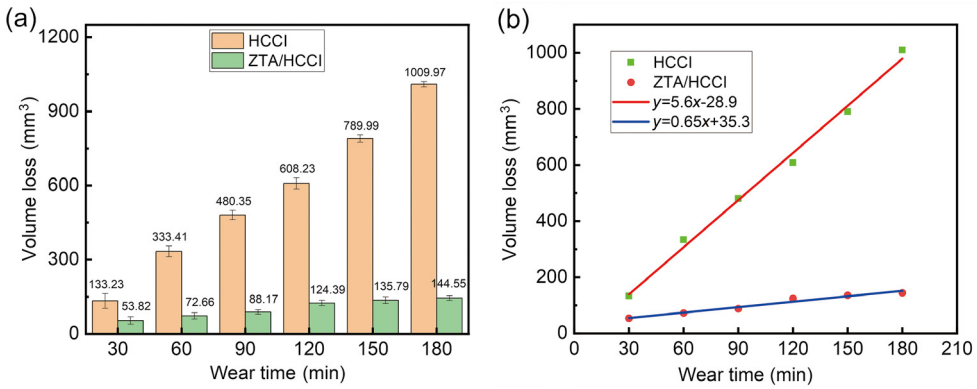

Fig. 14: Volume loss after different wear time (a), and wear volume-time relationship linear fitting (b)

As a result, the wear rate of the composite is decreased to 11.6% of HCCI. This clearly demonstrates that the ZTA/HCCI composite can effectively resist three-body abrasive wear. In other words, ZTA particles with Ni-B_4C plating can effectively improve the three-body wear resistance of HCCI.

Figure 15 shows the 3D morphology of pure HCCI and ZTA/HCCI composite wear surfaces. It is clear that the wear damage of the pure HCCI specimens is more severe than that of the composite specimens. The pure HCCI wear surface exhibits a long and deep parallel furrow morphology, as shown in Figs. 15(a and b). This is due to the fact that the quartz sand particles contain many sharp protrusions, and under high stress, the quartz sand particles will be extruded and embedded in the wear surface. Consequently, a long and deep parallel furrow presents on the wearing surface of the HCCI specimens. Furthermore, Fig. 16(a) shows the low magnification of HCCI wear surface morphology. The huge parallel furrows are clearly present on the wear surface of HCCI specimen, and there are microscopic micro-cutting marks between the furrows. It can be seen that the wear pattern of quartz sand abrasive on HCCI specimens is mainly plow cutting and micro cutting.

As shown in Figs. 15(c and d), the metal matrix depresses downward and the ceramic particles protrude on the wear surface of the composite specimen. The wear surface of the composite is substantially different from that of pure HCCI. This is primarily due to the formation of a chemically bonded interface layer (mainly comprised of ZrB_2, FeB, Fe_2B, $NaSiO_4$) in the composite between the ZTA particles and the metal matrix. The interface layer can improve interfacial wettability between ZTA and HCCI, resulting in the improvement of the composite's wear resistance. Consequently, the matrix metal of the composite will be firstly peeled off by abrasive plowing in the wear testing, followed by the interface layer grinding and finally the ceramic particles, resulting in an uneven wear surface of the composite. As shown in Fig. 16(b), the metal matrix that is not protected by ZTA particles is severely worn. These protected metal matrixes play an essential role in keeping the ZTA particles in place and preventing them from slipping out throughout the wear process. In conclusion, the designed interface layer between ZTA/HCCI strengthens ZTA's binding to the matrix metal and keeps ZTA firmly in place, lowering the possibility of flaking during wear.

Based on the aforesaid analysis, the wear mechanism of the composite material is depicted in Fig. 17. Before wearing, the ZTA particles are deeply embedded in the HCCI matrix. Because the interface layer enhances the wettability of the ZTA/HCCI interface, the result is a strong bond between ZTA and HCCI. At the beginning of wearing, the matrix metal on the surface directly contacts with the abrasive. As a result, the metal matrix is rapidly plowed, causing the ZTA particles to progressively protrude. Then, the ZTA particles begin to be ground owing to the rapid wear of the surrounding matrix metal. At the middle stage of wearing, the ZTA particles become the principal object of wear because they are relatively convex. The low wear rate and relative convexity of ZTA particles protect the matrix metal around the ZTA particles. At the same time, the interface layer between ZTA and HCCI

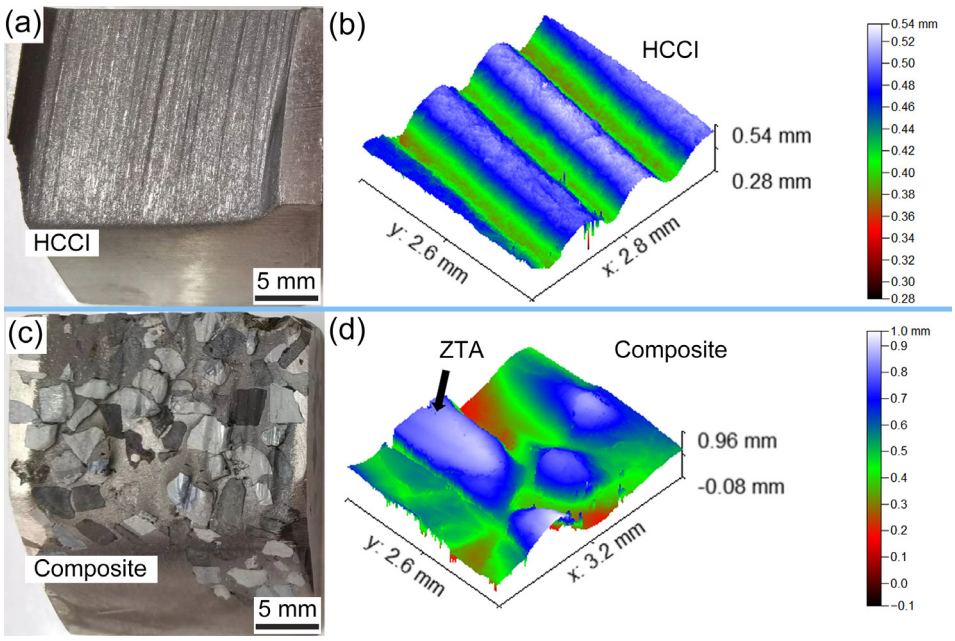

Fig. 15: Surface morphology after three-body wear test: (a) pure HCCI macro wear morphology; (b) pure HCCI 3D wear morphology; (c) composite macroscopic wear morphology; (d) composite 3D wear morphology

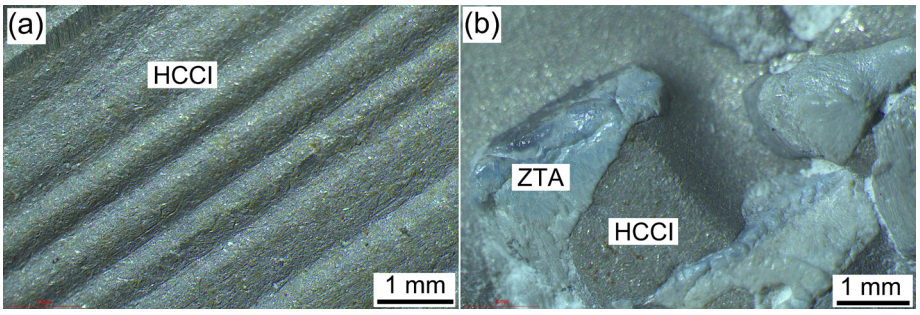

Fig. 16: Low magnification of HCCI and composite wear surface morphology: (a) HCCI; (b) composite

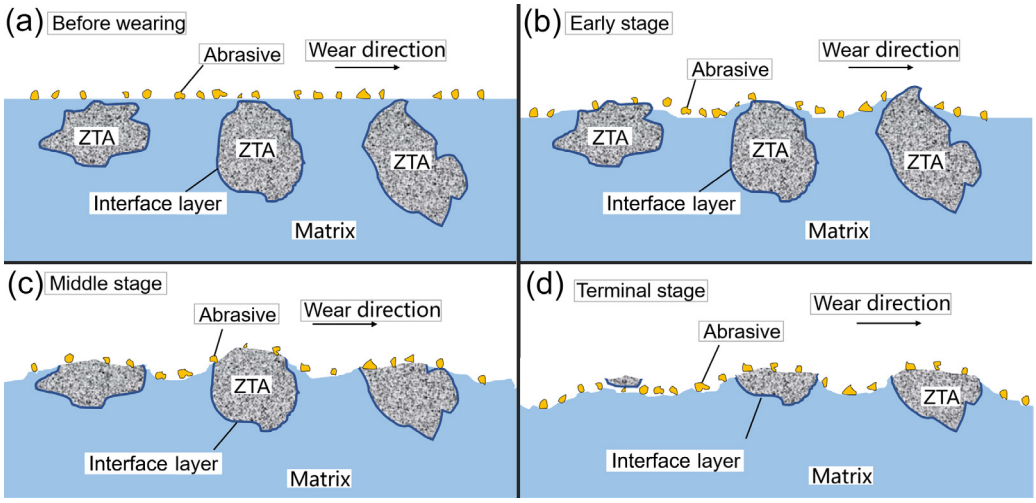

Fig. 17: Schematic diagram of wear resistance principle: (a) before wearing; (b) early stage; (c) middle stage; (d) terminal stage

strongly bonds the ZTA particles to the matrix metal and prevents them from falling off during the wearing process. At the end of wearing, the relatively convex ZTA particles are gradually depleted and even flaked off by persistent wear. The abrasive eventually comes into contact with the matrix metal again and begins a new round of wearing, and so on until the material is depleted.

4 Conclusions

(1) Surface-modified ZTA particles were prepared by chemical composite plating of Ni-B_4C, and the ceramic preforms were prepared by the plated ZTA and sodium silicate solution binder. The resulting preforms did not collapse during casting and infiltration of high-temperature HCCI liquid.

(2) At high-temperatures, ZrO_2 reacts with B_4C to form ZrB_2, B_4C reacts with Fe to form FeB and Fe_2B, which combine with the bonded residual $NaSiO_4$ to form a chemically bonded interface layer between the ZTA and HCCI interface. Furthermore, Ni elements diffuse in the metal matrix to form Ni-Fe solid solutions. As a result, the interfacial wettability between ZTA and HCCI is improved by the diffusion and reaction of Ni and B_4C.

(3) Between the ZTA/HCCI interface of the composite, a relatively soft interface layer is formed, and this interface layer can improve the wear resistance of the composites. During the three-body wear testing, the ZTA particles effectively block the abrasive cutting, and the wear rates of HCCI and ZTA/HCCI composite are 5.6 $mm^3 \cdot min^{-1}$ and 0.65 $mm^3 \cdot min^{-1}$, respectively. The wear rate of the ZTA/HCCI composite is decreased to 11.6% of HCCI.

Acknowledgements

This work was financially supported by the National Natural Science Foundation of China (52005217), the University Research Platform and Research Projects of Guangdong Education Department (2022ZDZX3003), Basic and Applied Basic Research Fund Project of Guangdong Province in China (2022A1515010091, 2021A1515010523, and 2020A1515110020), Basic Scientific Research Projects of Central Universities (No.21620344), and Jinan University Open Fund for Advanced Materials (JNIWRM2021004).

Conflict of interest

The authors declare that they have no known competing financial interests or personal relationships that could have appeared to influence the work reported in this paper.

References

[1] Ojala N, Valtonen K, Antikainen A, et al. Wear performance of quenched wear resistant steels in abrasive slurry erosion. Wear, 2016, 354–355: 21–23.
[2] Zhou M J, Jiang Y H, Sui Y D. Microstructure and properties of interfacial transition zone in ZTA particle-reinforced iron composites. Applied Physics A, 2019, 125(2): 110.
[3] Nikhilesh C, Krishan K. Metal matrix composites. New York: Springer New York Press, 2016.
[4] Zadorozhnaya O Y, Khabas T, Tiunova O, et al. Effect of grain size and amount of zirconia on the physical and mechanical properties and the wear resistance of zirconia-toughened alumina. Ceramics International, 2020, 46(7): 9263–9270.
[5] Banik S, Iqbal I, Nath R, et al. State of the art on zirconia toughened alumina cutting tools. Materials Today: Proceedings, 2019, 18: 2632–2641.
[6] Dong Q, Xing S M, Qiu B. Mixed regulation model of ceramic particles with molten high-chromium iron KmTBCr26. China Foundry, 2019, 16(2): 135–140.
[7] Bhide S V. Wear-resistant metal matrix ceramic composite parts and methods of manufacturing thereof. US: US8147980B2, 2012-04-03.
[8] Ma X, Li L F, Zhang F, et al. Microstructure and wear characteristics of ATZ ceramic particle reinforced gray iron matrix surface composites. China Foundry, 2018, 15(3): 167–172.
[9] Ru J, He H, Jiang Y, et al. Wettability and interaction mechanism for Ni-modified ZTA particles reinforced iron matrix composites. Journal of Alloys and Compounds, 2019, 786: 321–329.
[10] Ru J, He H, Jiang Y, et al. Ionic liquid-assisted preparation of Ni-Cr dual wrapped ZTA particles for reinforced iron-based composites. Advanced Engineering Materials, 2019, 21(5): 1801120.
[11] Fan L, Wang Q, Yang P, et al. Preparation of nickel coating on ZTA particles by electroless plating. Ceramics International, 2018, 44(10): 11013–11021.
[12] Terry B, Chinyamakobvu O. Assessment of B_4C reaction with liquid iron alloys. Journal of Materials Science, 1994, 29(2): 464–467.
[13] Gao Q, Lu Z, Jia L, et al. Effect of B_4C on bending strength of ZTA ceramic reinforced high chromium cast iron matrix composites. Composite Interfaces, 2022, 29(8): 971–983.
[14] Aizenshtein M M I, Froumin N. Interface interaction in the B_4C/(Fe-B-C) system. Materials Science and Engineering: A, 2008, 495(1–2): 470–474.
[15] Ozkan V I H S, Erol A. Influence of mean grain size with ultrasonic velocity on microhardness of B_4C-Fe-Ni composite. Journal of Alloys and Compounds, 2013, 574: 512–519.
[16] Zhao H, He Y, Jin Z. Preparation of zirconium boride powder. Journal of the American Ceramic Society, 1995, 78(9): 2534–2536.
[17] Li Y J. Ceramic metal composite materials. Beijing: Metallurgical Industry Press, 2004. (In Chinese)
[18] Zhou M J, Jiang Y H, Wen F F, et al. Influence of heat treatment on the wear resistance of high chromium cast iron based honeycomb ceramic composites. Materials Reports, 2017, 31(14): 117–121. (In Chinese)
[19] Zheng K, Gao Y, Li Y, et al. Three-body abrasive wear resistance of iron matrix composites reinforced with ceramic particles. Proceedings of the Institution of Mechanical Engineers, Part J: Journal of Engineering Tribology, 2014, 228(1): 3–10.
[20] Araghi A, Paydar M. Electroless deposition of Ni-P-B_4C composite coating on AZ91D magnesium alloy and investigation on its wear and corrosion resistance. Materials & Design, 2010, 31(6): 3095–3099.
[21] Fan L, Wang Q, Yang P, et al. Preparation of nickel coating on ZTA particles by electroless plating. Ceramics International, 2018, 44 (10): 11013–11021.
[22] Krukovich M G, Prusakov B A, Sizov I G, et al. The equilibrium diagram of 'boron-iron' binary system. Plasticity of Boronized Layers, 2016: 23–38.
[23] Miao M C, Chen Y. College physics experiments. Beijing: Beijing University of Aeronautics and Astronautics Press, 2018. (In Chinese)
[24] Sui Y, Zhou M, Jiang Y. Characterization of interfacial layer of ZTA ceramic particles reinforced iron matrix composites. Journal of Alloys and Compounds, 2018, 741: 1169–1174.